INTERNATIONAL JOURNAL OF AUTOMOTIVE AND MECHANICAL ENGINEERING
ISSN: 2229-8649 e-ISSN: 2180-1606
VOL. 22, ISSUE 1, 2025, 12118 – 12132
DOI: https://doi.org/10.15282/ijame.22.1.2025.13.0930

RESEARCH ARTICLE

Machine Learning-Based Prediction of Impact Toughness in AISI 430–AISI 304 Friction-Welded Joints

Jagadesh Kumar Jatavallabhula[1]*, Vasudeva Rao Veeredhi[1], Gundeti Sreeram Reddy[2], Ravinder Reddy Baridula[2], Vaddi Venkata Satyanarayana[2]

[1]Department of Mechanical, Bioresources and Biomedical Engineering, College of Science, Engineering and Technology, University of South Africa, Florida Campus, Johannesburg, South Africa

[2]Department of Mechanical Engineering, Vidya Jyothi Institute of Technology, Aziznagar, Hyderabad, India

ABSTRACT – Friction welding is a solid-state joining technique widely used for dissimilar materials due to its efficiency and cost-effectiveness. However, welding AISI 430 ferritic and AISI 304 austenitic stainless steels poses challenges due to their differences in chemical composition and mechanical properties, particularly in achieving optimal impact toughness. Existing studies focus on optimizing process parameters but lack predictive modeling for impact toughness using machine learning (ML). This study aims to bridge this gap by experimentally evaluating the impact toughness of friction-welded AISI 430–AISI 304 joints and developing ML models for accurate prediction. Experiments were designed using a Taguchi L_{32} orthogonal array, varying friction force, forge force, and burn-off. Charpy impact tests were performed to assess toughness, and the results were used to train Decision Tree, Random Forest, and Gradient Boosting regression models. Random Forest regression outperformed others with an R^2 value of 0.98 and a mean squared error of 0.29. The predicted impact toughness (15.8 J) closely matched the value from the confirmation experiment (16 J) with only a 1.25% deviation. The findings demonstrate that ML can significantly enhance process optimization, reducing reliance on costly experimental runs. Future research should explore additional welding parameters and deep learning models for further improvements.

ARTICLE HISTORY
Received : 19th Oct. 2024
Revised : 23rd Jan. 2025
Accepted : 11th Feb. 2025
Published : 12th Mar. 2025

KEYWORDS
Friction welding
Impact toughness
Machine learning
Random forest
Taguchi analysis

1. INTRODUCTION

Friction welding (FW) is a procedure in which two materials are joined by generating frictional heat, with no melting of the materials. Successful FW of dissimilar materials is an arduous task owing to the disparities in chemical compositions and mechanical properties, which profoundly affect the quality of the joints [1, 2]. Impact toughness evaluation of dissimilar joints is vital for understanding their behavior under loads, especially in this era where the demand for combining different materials is growing in industries [3]. Emami et al. researched the friction stir welding (FSW) of dissimilar AISI 430 and AISI 304L steels to find the optimum process variables to ensure the production of high-quality joints and emphasized that microstructural changes, such as dynamic recrystallization, led to increased hardness and tensile strength in the weld zone. Their research highlighted the importance of accurately controlling heat and tool offset to achieve superior quality in welded joints [4]. The microstructural characteristics and mechanical properties of similar/ dissimilar welds of stainless steel using electron beam welding (EBW) and FW were compared by Madhusudan Reddy et al. It was found that EBW produced precise, high-quality welds with minimal heat-affected zones and superior tensile strength, although it had the disadvantage of being expensive and complex. FW was proposed as a more cost-effective and suitable option for solid-state joining, particularly dissimilar metals, though it yielded relatively inferior strength and toughness. Finally, it was concluded that EBW is ideal for high-performance applications, while FW is economical for less demanding tasks [5].

Impact toughness measures a material's capacity to absorb energy and deform without fracturing. In friction welded joints, factors like weld microstructure, defects, and residual stress affect this property. Traditional testing methods like Charpy impact tests assess impact toughness but are often slow and resource-intensive. Recent advancements in machine learning (ML) offer efficient predictions of material properties, making them a valuable tool for evaluating impact toughness in welded joints, particularly in dissimilar stainless steel. This approach streamlines the process, saving time and resources while focusing on how weld microstructures influence toughness [6]. Zambrano et al. reviewed the impact of fracture toughness and impact toughness on impact-abrasion wear in mining industries. They highlighted that previous research primarily focused on hardness improvements while neglecting the role of toughness in mitigating wear. The authors systematically analyzed existing studies, emphasizing the complex interaction between toughness and wear mechanisms [7]. Kim et al. introduced a novel surface-cracking method to enhance the strength and impact toughness of cold-worked austenitic stainless steels, specifically for cryogenic environments. The study demonstrated that combining cold working with surface cracking effectively enhanced the strength and toughness of austenitic stainless steels while

*CORRESPONDING AUTHOR | Jagadesh Kumar Jatavallabhula | ✉ jagadeshkumar82@gmail.com

preserving their ductility [8]. Hou et al. investigated the impact toughness of 100 mm ultra-thick offshore steel, which was welded by employing narrow gap laser wire filling welding at low temperatures.

It was found that the weld surface exhibited good impact toughness comparable to the base material, while the weld core showed reduced toughness due to grain coarsening. The viability of this welding method for joining ultra-thick steel plates was proved in the work [9]. Luo et al. examined the microstructure and impact toughness of TC4 titanium alloy joints welded using laser-arc hybrid methods and observed that the weld showed a basket-weave α martensite structure, with Widmanstatten structures in upper layers reducing toughness. Peak hardness reached 420 HV in cosmetic layers, and impact toughness was 91.3% of the base metal, influenced by porosity and grain size variations. The study emphasized the need for optimizing welding parameters to enhance toughness [10]. Tunçel optimized the Charpy impact strength of PLA fabricated by fused deposition modeling by employing the Taguchi method and found that infill density and print speed were the most critical parameters, accounting for 38.93% and 36.51% of the influence, respectively. It was reported that the optimized parameter combination enhanced impact strength by 1.39%, reaching 38.54 kJ/m^2 [11]. Saleh et al. conducted a multi-objective optimization study on the FSW of AA5754 alloy, using the Taguchi method and grey relational analysis to optimize tensile strength, hardness, and impact toughness. The ANOVA results showed that tool rotation speed contributed most significantly to these properties, followed by traversal rate and tilt angle. The optimal parameters were determined to be tool rotation at 1000 rpm, traversal rate of 60 mm/min, and a tilt angle of 2.5º [12]. Safeen et al. built mathematical models to predict tensile strength, impact toughness, and hardness of FSW AA6061 joints employing response surface methodology and concluded that the tool pin profile was the most significant factor affecting mechanical properties, with simple cylindrical pin profiles yielding superior results. Optimal parameters condition achieved 92% of the UTS, 87% of the impact toughness, and 95% of the hardness when compared to the base material [13].

ML algorithms can accurately predict the impact toughness of weld joints, reducing the need for costly experimental testing and enabling continuous process optimization. This technology enhances the quality, reliability, and efficiency of stainless-steel friction-welded joints, as demonstrated by research findings [14]. ML models trained on friction-welded joints with known impact toughness can predict toughness for new joints based on input parameters. Geng Chen et al. employed an ML parallel approach with Principal Component Analysis for dimensionality reduction and K-means for clustering, outperforming conventional back propagation neural networks in prediction accuracy [15]. Yimian Chen et al. applied ML to enhance Charpy impact toughness (CIT) in low-alloy steel by recognizing key material descriptors. It was discovered that the Random Forest method was the most accurate relative for CIT predictions. Further, a genetic programming-based symbolic regression provided a formula to link features to CIT, paving a path to develop high-toughness, low-alloy steel for engineering applications [16]. Si-Wei Wu et al. developed a scheme to predict Charpy V-notch impact energy in low-carbon steel by applying neural network models. Extreme learning machine (ELM), three-layer neural network, and deep neural network (DNN) were compared using industrial data of chemical constituents and process variables. It was reported that the DNN model, optimized with Bayesian hyper-parameter tuning, outperformed the others [17]. Yupeng Diao et al. developed five ML-based models to predict several properties of carbon steels. Support vector regression (SVR) with radial basis function kernel and multi-layer perceptron (MLP) were concluded to be the most efficient in predicting mechanical properties [18]. Shaban et al. used ML to examine the impact of Equal Channel Angular Pressing (ECAP) on the mechanical and electrical properties of pure copper. Linear regression, regression trees, and artificial neural networks were employed in the study, and it was concluded that ECAP increased the mechanical strength of copper without significantly reducing its electrical conductivity. Besides, the ANN model produced the most accurate predictions based on ECAP parameters [19].

Junhak Pak et al. optimized the neural networks approach to enhance toughness in steel welds and assessed the effects of processing on strength and ductility in low-carbon automotive steels. Finally, successful neural network optimization was achieved for accurate predictions of toughness [20]. The application of ML for the design, phase transformation, and mechanical properties of alloys was comprehensively reviewed by J.F. Durodola et al., who highlighted the capability of ANN to model complex, non-linear relationships in materials science. The effectiveness of ML techniques in predicting phase transformations was also highlighted [21]. Stoll et al. researched the use of ML techniques for material characterization, with a special focus on predicting mechanical properties from small punch test (SPT) data. A strong correlation between SPT results and conventional tensile tests was identified, and ML models such as Random Forest (RF) and linear regression were suggested as promising means to predict ultimate tensile strength (UTS), thereby reducing the need for conducting time-consuming and costly mechanical tests [22]. Guo et al. reviewed the applications of ML in material science and showcased how ML techniques can predict material properties and optimize complex designs. The authors also highlighted key inventions in ML-based material design that can help overcome conventional limitations. Furthermore, open challenges and prospects in the field were discussed, encouraging more progress in this emerging area [23]. Smyrnov et al. applied ensemble learning and data augmentation techniques to predict the material toughness in additively manufactured metallic parts. ML models like Random Forest and boosting algorithms were employed to enhance the predictive accuracy based on limited data. The efficiency of ML methods in optimizing toughness in additive manufactured components was proved [24]. Xu et al. built an ML model to predict the impact toughness of cast austenitic steel that yielded an R-squared value of 0.965 and was in minor deviation from the measured values [25].

Although dissimilar FW of AISI 430 and AISI 304 stainless steels is increasingly applied, most existing research has concentrated on optimizing welding parameters and evaluating mechanical properties like tensile strength and hardness.

However, there has been a notable lack of studies systematically predicting the impact toughness of these joints using ML techniques. Thus, a critical gap exists in the application of ML models specifically designed to predict the impact toughness of dissimilar FW stainless steel (SS) joints. Bridging this gap with ML models could significantly reduce both the time and cost associated with experimental methods, offering a more efficient and scalable approach to estimating impact toughness in dissimilar stainless steel welds. This is vital due to the critical role impact toughness plays in warranting the integrity of welded joints.

The primary objectives of this research are to evaluate the impact toughness of dissimilar friction-welded joints of the chosen steels, analyze the results using the Taguchi method to optimize key welding parameters and build ML models for highly accurate predictions of impact toughness. Decision Tree, Random Forest, and Gradient Boosting models will be employed to predict impact toughness based on key parameters, including friction force, forge force, and burn-off. The study will evaluate the predictive accuracy of these models and assess their potential to reduce experimental costs while improving welding process optimization for industrial applications. The research work undertaken is illustrated as a flowchart in Figure 1.

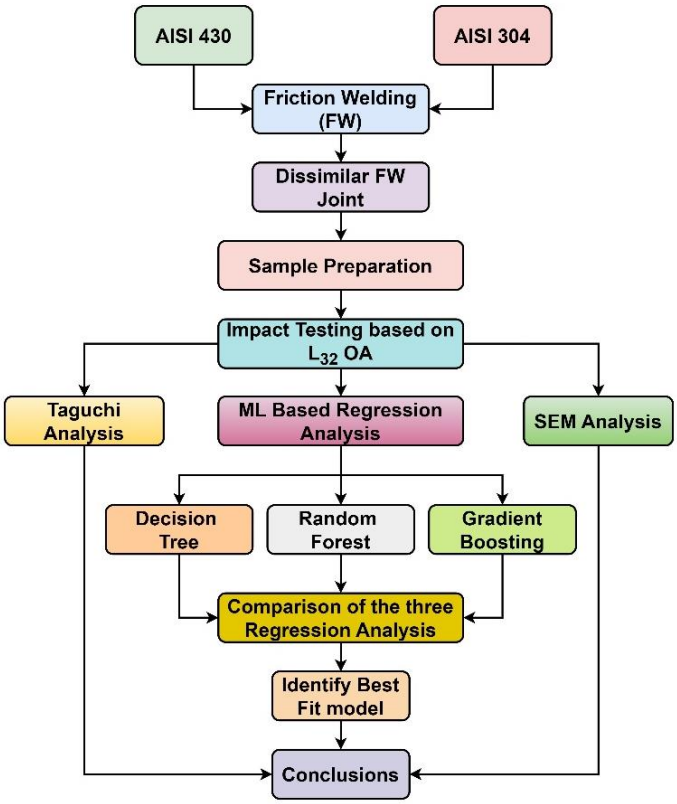

Figure 1. Flowchart of the work

2. METHODS AND MATERIAL

2.1 Materials

AISI 430 ferritic SS comprises elongated ferrite grains with carbides along the grains, while the AISI 304 austenitic SS comprises austenite grains that are equiaxed with prevalent twining, as shown in Figure 2. The chemical composition and mechanical properties of the materials undertaken are presented in Tables 1 and 2 respectively.

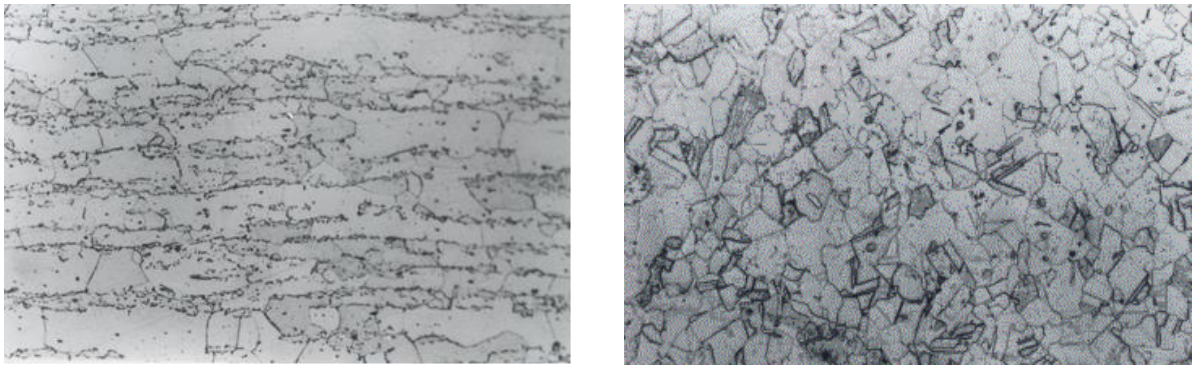

(a) (b)

Figure 2. Microstructures (a) AISI 430, (b) AISI 304

Table 1. Chemical composition (wt%)

Element/ Steel	Cr	Mn	Si	Ni	C	P	S	Fe
AISI 430	17.0	0.4	0.4	-	0.06	0.04	0.03	Balance
AISI 304	18.4	1.38	0.32	8.17	0.06	0.4	0.28	Balance

Table 2. Mechanical properties

Steel	% Elongation	Yield strength (MPa)	Ultimate tensile strength (MPa)	Hardness (HBW)	Impact Toughness (J)
AISI 430	28	380	488	197	14
AISI 304	58	250	600	227	132

Thermal conductivity plays a vital role in friction welding as it governs the heat transfer between the materials. It is 26.1 W/mºK for AISI 430 and 16.2 W/mºK for AISI 304.

2.2 Friction Welding

FW involves no melting of the joining metals, and the weld zone experiences thermo-mechanical working that causes a consolidated joint in a noticeably brief time. A continuous drive FW machine with 150 kN capacity and ETA was employed to weld the rods of the selected materials. The machine can adjust rotational speed from 0 to 2400 rpm and modify friction force, forge force, and burn-off to create joints with various parameter combinations. The machine headstock spindle, driven by an AC servomotor, holds one piece while the tailstock holds the other piece to be joined and made to traverse on the bed guideways. The pressure and displacements are controlled through a closed-loop control system during the welding process. Two rods of 18 mm diameter are taken by fixing one in the headstock and the other in the tailstock. The headstock rod rotates at a controlled speed, generating heat through friction with the stationary tailstock rod, softening the material for forging. The tailstock rod applies axial pressure, enhancing the bond strength while maintaining alignment and stability. Proper control of rotational speed and pressure is essential for optimal weld quality. The burn-off material during the process comes out in the form of a flash, and a typical friction welded joint is presented in Figure 3. The macrostructure of the joint is presented in Figure 4, along with an illustration of both the materials and the flash.

Figure 3. Dissimilar Joint after friction welding, A: austenitic steel, F: ferritic steel

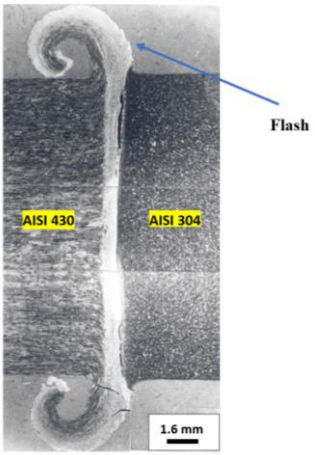

Figure 4. Macrostructure of joint

2.3 Experimental Design

FW parameters employed in the current research are shown in Table 3, and the experiments were designed using the Taguchi L_{32} orthogonal array with three factors, X1, X2 and X3, at two levels each. Taguchi method is undertaken as it enables to reach optimality with reduced experimental investigations. The L_{32} orthogonal array is presented in Table 4,

and the response investigated is Impact Toughness in Joules. Trial runs were initially conducted to ensure defect-free joints and finalize the parameters' ranges. Delaminations and defects were identified in the welded joints during the inspection when welding was carried out with the parameter values outside the chosen domain.

Table 3. FW parameters

S. No.	Parameter (Notation)	Units of measurement	Low level	High level
1	Friction Force (X_1)	kN	4	6
2	Forge Force (X_2)	kN	8	12
3	Burn-off (X_3)	mm	3	5

Table 4. L_{32} orthogonal array for impact toughness testing

Run	X1	X2	X3	Run	X1	X2	X3
1	4	8	3	17	6	8	3
2	4	8	3	18	6	8	3
3	4	8	3	19	6	8	3
4	4	8	3	20	6	8	3
5	4	8	5	21	6	8	5
6	4	8	5	22	6	8	5
7	4	8	5	23	6	8	5
8	4	8	5	24	6	8	5
9	4	12	3	25	6	12	3
10	4	12	3	26	6	12	3
11	4	12	3	27	6	12	3
12	4	12	3	28	6	12	3
13	4	12	5	29	6	12	5
14	4	12	5	30	6	12	5
15	4	12	5	31	6	12	5
16	4	12	5	32	6	12	5

2.4 Impact Toughness Testing

Impact testing of the specimens was conducted at room temperature using a Tinius Olson (TO) machine. The specimen was cut from the weldment with its axis oriented perpendicular to the joint, and the notch was positioned at the center of the weld, as depicted in Figure 5. A sample specimen after fabrication is presented in Figure 6.

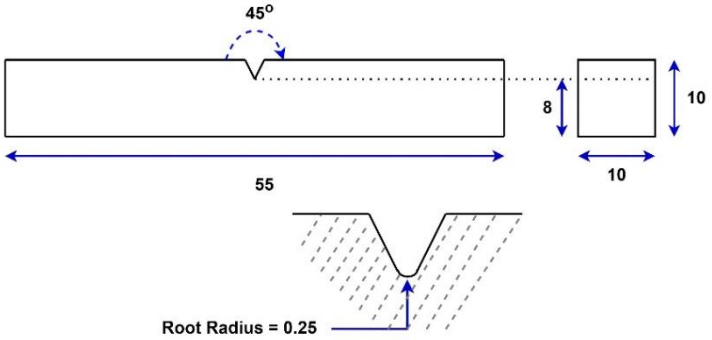

Figure 5. Schematic of the impact specimen

Figure 6. Specimen after fabrication

2.5 Scanning Electron Microscopy

Scanning Electron Microscopy (SEM) is used to inspect the fractured features from the failed specimens at various magnifications. Samples of appropriate sizes are machined, ultrasonically cleaned and degassed before being placed into the SEM chamber for examination. The Zeiss Crossbeam 550 SEM integrates advanced imaging with focused ion beam technology and is utilized for high-resolution imaging and microstructure analysis.

2.6 Machine Learning-Based Regression Analysis

ML-based regression analysis involves using algorithms to predict continuous outcomes by modeling the relationship between input features and target variables [26]. This approach helps identify patterns and optimize parameters for accurate predictions, reducing the need for extensive experimental data. It is useful in design engineering to predict mechanical properties like impact toughness from process parameters. Three regressions, namely Decision Tree, Random Forest and Gradient Boosting, are developed and investigated in the current research. The ML models are programmed in Python by leveraging libraries like Numpy, Pandas, Matplotlib and Sklearn.

2.6.1 Decision Tree Regression

Decision Tree Regression (DTR) is a non-parametric supervised ML algorithm employed to predict continuous outcomes, and it works on the principle of splitting data into smaller subsets based on input features. At each node, it chooses a feature and value that best separates the data, using a loss function like MSE to establish the optimal split. This continues recursively till a stop criterion, such as maximum depth or minimum samples per node, is met. The major advantages of DTR are its ease of use and interpretability. Each node denotes a specific condition, making the model easy to understand and visualize [27]. It can also capture non-linear relationships between variables, making it handy for various regression activities. Nevertheless, deep trees can overfit the training data, lowering performance on new data. To prevent overfitting, procedures like pruning or hyperparameter tuning (e.g., maximum depth, minimum samples per split) are employed. The performance of the model is measured using metrics like MSE and R-squared. In the current research, the hyperparameter that is tuned in DTR is the 'max depth', which represents the longest pathway between the root node to a leaf node, determining how many times the tree can split before stopping. In short, the steps in DTR include data preprocessing, tree construction, recursive splitting, prediction at leaf nodes, evaluation of the model, tuning of hyperparameters, and final prediction.

2.6.2 Random Forest Regression

Random Forest (RF) regression is an ensemble technique, and it predicts continuous variables by building numerous decision trees on subsets of data and features selected at random. The randomness in data and feature selection aids in reducing overfitting, and the final predicted value is the average of outputs of all trees. This approach provides more robust and accurate results than relying on a single decision tree. RF is very good at handling complex interactions and non-linear relationships between variables. By taking the average of multiple tree predictions, RF lowers the variance and averts the model from being overly sensitive to specific data points. RF model can handle missing data gracefully and requires minimal preprocessing [28]. Tuning hyperparameters, like the number of trees and tree depth, is critical for optimizing the performance of the model. RF also ranks feature importance in identifying the most influential variables, thereby making the model accurate and interpretable. In short, the steps in RF regression include preprocessing the data, building multiple decision trees, training the forest using bootstrapped data samples, making predictions by averaging the outputs of the discrete trees, evaluating the performance, tuning the hyperparameters to improve the accuracy, and final prediction.

2.6.3 Gradient Boosting Regression

Boosting Regression (GBR) is an ensemble ML approach that constructs models step-by-step by adding decision trees in sequence to reduce the errors in prediction. The process starts with an initial model, often a shallow decision tree or a constant value. Then, the residuals are computed, and a new decision tree is trained to correct these residuals. This process recurs, with each new tree's contribution adjusted by a learning rate (η) until the model achieves the desired accuracy. In each iteration, the overall prediction is revised by adding the outputs of all the preceding trees. Important hyperparameters, such as the "no: of trees", "learning rate" etc., are adjusted throughout for performance optimization. The final prediction is the aggregate sum of the outputs of all individual trees [29]. The accuracy of the model is assessed through metrics like Mean Squared Error (MSE) and R-squared (R^2), which measure how efficiently the model applies to new data. GBR is an excellent option for handling complex relationships, and the incremental refinement of predictions gives good results. However, cautious tuning of hyperparameters is vital to avoid overfitting and to get reliable predictions. In short, GBR starts with initializing a simple model and calculating residual errors. A new model is then fitted to these residuals, and the process is iteratively repeated to update the model. Subsequently, model evaluation and tuning of hyperparameters are performed to make the final predictions.

2.6.4 Mean Squared Error

Mean Squared Error (MSE) is the average of the squared differences between the investigational values and the anticipated values from the ML model. The smaller magnitude of MSE indicates that the predicted values are closer to

the actuals, representing a better fit. MSE becomes critical when the magnitude of the average error and its impact are to be known [30]. MSE can be computed from the formula mentioned in Eq. 1.

$$MSE = \frac{1}{n}\sum_{i=1}^{n}(y_i - \hat{y}_i)^2 \quad (1)$$

where:

n represents the no. of data points

y_i represents the actual value for the experiment, and

$\hat{y}_i$ is the value obtained from the prediction

2.6.5 R-squared

R-squared (coefficient of determination) signifies the variance in the dependent variable that is predicted from the independent variable(s). It is a relative measure of how efficiently the model explains the variance in the data, making it simpler to interpret the performance of the model [31]. R-squared = 1 denotes a perfect fit, and R-squared = 0 suggests that the model lacks predictive accuracy and should be revised. R-squared can be negative when the model is poorer than merely treating the mean as a predictor, and this represents a very poor model fit [32]. The formula for computing R-squared is mentioned in Eq. 2.

$$MSE = \frac{1}{n}\sum_{i=1}^{n}(y_i - \hat{y}_i)^2 \quad (1)$$

$$R - Squared = 1 - \frac{SS_{res}}{SS_{tot}} \quad (2)$$

where:

SS_{res} represents the residual sum of squares computed from Eq. 3.

$$SS_{res} = \sum_{i=i}^{n}(y_i - \hat{y}_i)^2 \quad (3)$$

SS_{tot} represents the total sum of squares computed from Eq. 4.

$$SS_{tot} = \sum_{i=i}^{n}(y_i - \bar{y}_i)^2 \quad (4)$$

$\bar{y}_i$ in Eq. 4 is the mean of the actual values.

3. RESULTS AND DISCUSSION

Compared to AISI 430 ferritic SS, AISI 304 austenitic SS possesses lower thermal conductivity, higher hardness and superior strength. Consequently, during friction welding, AISI 304 experienced less deformation, resulting in more burn-off flash on the AISI 430 side (Figure 4) [33]. Due to this reason, the friction welded joint exhibited properties, specifically impact toughness, more aligned towards AISI 430. The microstructural characteristics of the FW joint are presented in Figure 7. A comparison between Run 14 (high impact toughness) and Run 22 (low impact toughness) reveals substantial variations in the microstructural morphology. Run 14, which demonstrates higher impact toughness, shows a more homogeneous grain structure with refined grains in the ferritic phase, contributing to improved energy absorption during impact loading. On the contrary, Run 22, with lower impact toughness, displays coarser grains with incomplete recrystallization, resulting in localized stress concentration and reduced ductility. The observed microstructural transitions confirm the significant influence of FW parameters on the weld quality. Higher forging force and burn-off levels cause extensive dynamic recrystallization and refined microstructures, leading to superior impact toughness, whereas lower levels result in insufficient grain refinement, reducing the joint's toughness.

Figure 8 presents the micrograph of the FW joint at the weld centerline (Run 13), highlighting the transition zone between the AISI 430 and AISI 304. The intense thermo-mechanical effects induced by FW caused the microstructural evolution at the weld interface. At the weld center, a diffusion-driven transition zone is observed, characterized by the intermixing of ferritic and austenitic phases. This region exhibits a gradient in grain morphology, changing from fine equiaxed grains in the ferritic region to elongated austenitic grains. On the left side of the interface, AISI 304 exhibits parallel bands, while on the right side, an equiaxed grain structure is observed in AISI 430, owing to the dynamic recrystallization that occurred during the process of welding. Further, the grains appear bent and elongated on the right side. The formation of these parallel bands on the austenitic side or the bent grains on the ferritic side can be attributed to the tangential forces generated by the applied torque during welding. The welded joints' impact toughness results are presented in Table 5, and they are in the range of 15-27 J, with the highest toughness achieved when the forging force was at its maximum. The metals were heated by friction between the faying surfaces and securely bonded with a high

forging force, resulting in a strong joint. Toughness is influenced by the heat generated from friction and the distribution of that heat, leading to greater burn-off and increased time for the heat to spread. This condition stabilizes the microstructure and enhances toughness.

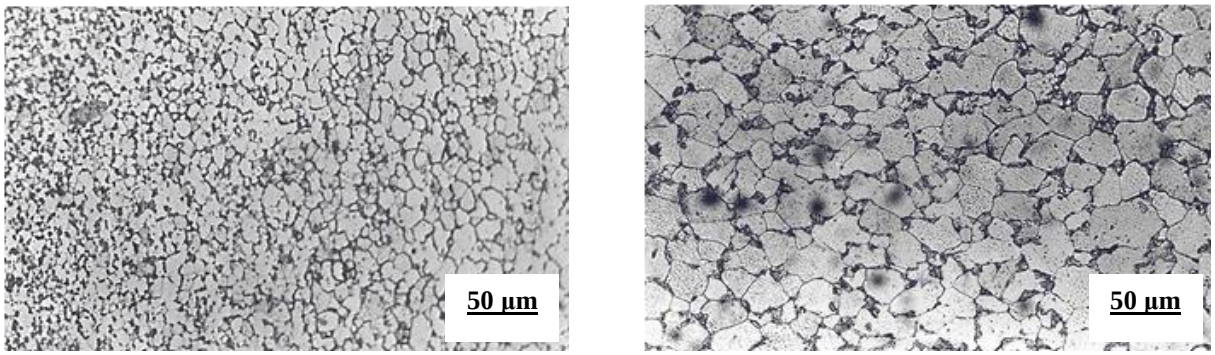

(a) Run 14 (high impact toughness) (b) Run 22 (low impact toughness)

Figure 7. Microstructure of the FW welded joint

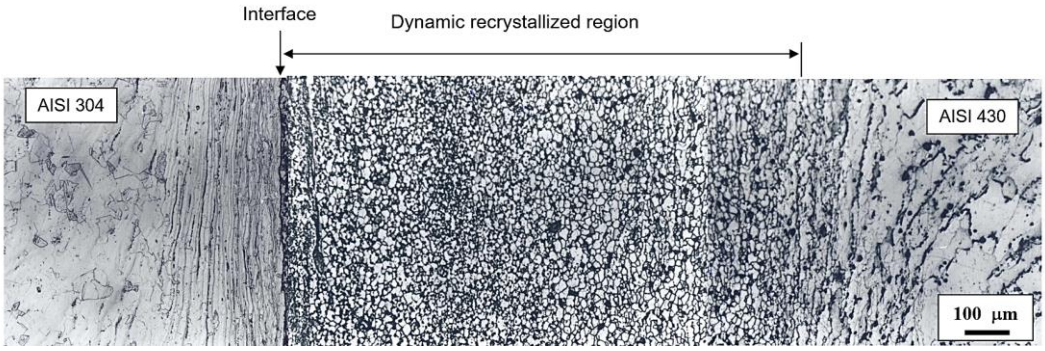

Figure 8. Typical micrograph of a dissimilar friction weld at the center (Run 13)

The fractography of the toughness specimen confirms this by displaying a high-energy ductile micro-void fracture, as shown in Figure 9. The high-impact toughness specimen shows fracture characteristics that include micro-voids (Figure 9(a)) indicating a ductile fracture, whereas the low-impact toughness specimen, the fracture exhibits cleavage features (Figure 9(b)), indicating a brittle fracture due to lack of plasticity and consequent rapid crack propagation. The micrographs presented in Figure 7-9 reiterate the fact that fine-grained, dynamically recrystallized weld microstructures exhibit superior impact toughness, whereas coarse-grained, unrefined structures lead to brittle failure. This underscores the necessity of carefully regulating welding parameters to ensure superior weld quality in dissimilar SS friction welds.

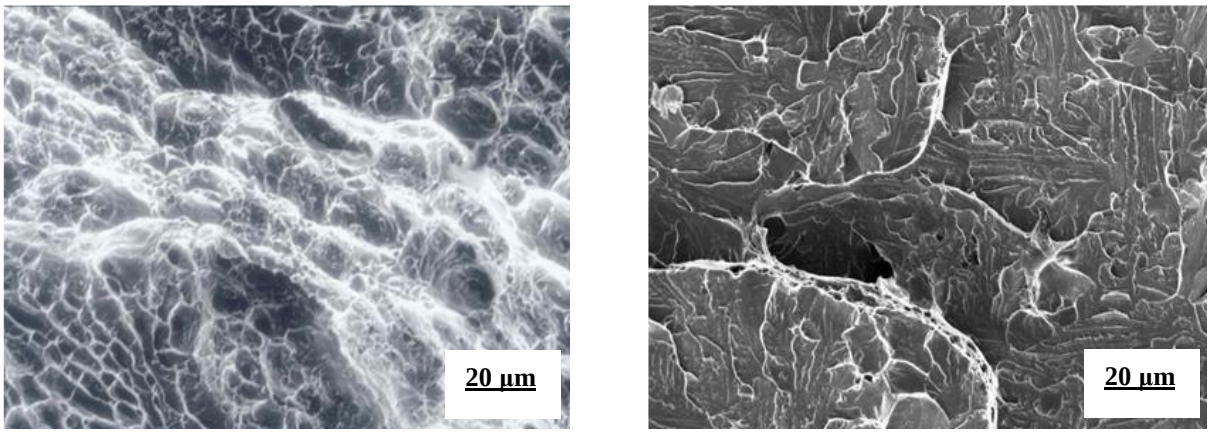

(a) Run 14 (high impact toughness) (b) Run 22 (low impact toughness)

Figure 9. Fractography of the toughness specimens

3.1 Impact Toughness Experimental Results

The impact toughness results for the chosen welded joints are illustrated in Table 5, and they range between 15 and 27 Joules. It is maximum, i.e., 27 Joules for Run 14 and Run 16, where the forge force is at the maximum level, and it is lowest, i.e., 15 Joules for Run 1 and Run 22, where the forge force is at the minimum level. Taguchi analysis can give further insight into the optimality of parameters.

Table 5. Impact toughness of the welded joints

Run	Impact Toughness (Joules)	Run	Impact Toughness (Joules)
1	15	17	18
2	16	18	19
3	16	19	18
4	17	20	19
5	18	21	16
6	19	22	15
7	19	23	17
8	20	24	17
9	16	25	21
10	17	26	20
11	18	27	19
12	17	28	20
13	25	29	24
14	27	30	24
15	26	31	23
16	27	32	25

3.2 Taguchi Analysis of the Results

The toughness results from various combinations of friction welding parameters were analyzed using Analysis of Means (ANOM), as shown in Table 6, with the corresponding graphical representation in Figure 10. The analysis indicates that the optimal toughness is achieved when all welding parameters are set to their maximum levels. Parameters X1, X2, and X3 contribute 0.04% to 4.17% individually, but their interactions, particularly X1*X3 and X2*X3, significantly affect outcomes, i.e. 13.73% and 19.46%. This suggests that burn-off reduces heat from friction and forge forces, leading to increased impact toughness when these parameters are high [34, 35].

Table 6. Response for means

Level	X1	X2	X3
1	19.56	17.44	17.88
2	19.69	21.81	21.38
Delta	0.13	4.38	3.50
Rank	3	1	2

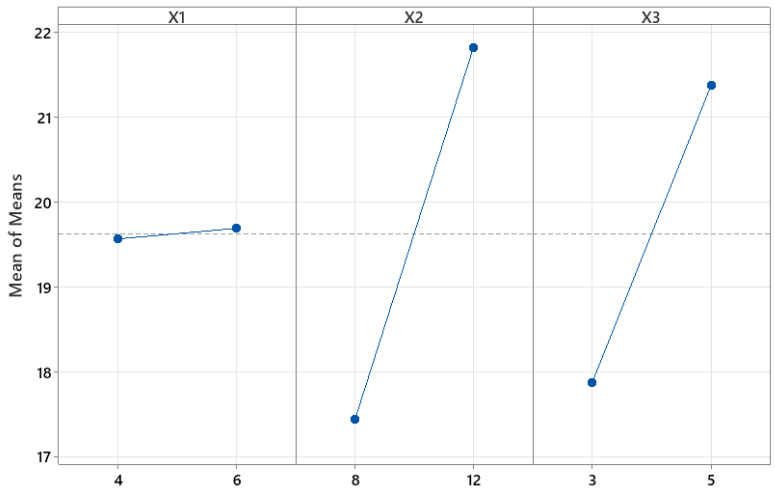

Figure 10. ANOM plot for maximizing the impact toughness

The higher contributions of X1 and X2 can be attributed to their direct influence on heat generation and material flow during FW. Friction force (X1) is responsible for producing heat at the interface, which influences the softening and plastic deformation of the materials being welded. Similarly, forge force (X2) plays a dominant role in consolidating the joint, ensuring that the softened material is properly forged to remove defects, reduce porosity, and refine the

microstructure. In contrast, burn-off (X3) has a lower contribution (0.04%), indicating that its impact on toughness is secondary compared to X1 and X2. The relatively minimal contribution of burn-off suggests that as long as sufficient material displacement occurs to form a defect-free joint, its variations have a limited effect on impact toughness. The greater effect of X1*X3 and X2*X3 interactions on impact toughness can be attributed to the synergistic effects of frictional heat, plastic deformation, and controlled material displacement, which collectively dictate microstructural evolution and defect elimination. In contrast, X1*X2 has a negligible effect because friction and forge forces operate in different welding phases and do not interact in a manner that significantly alters toughness.

Table 7. Results of ANOVA

Source	DF	SS	MS	% Contribution
Regression	6	385	64.1667	
X1	1	16.741	16.7411	4.17
X2	1	16.741	16.7411	4.17
X3	1	0.157	0.1569	0.04
X1*X2	1	0.5	0.5	0.12
X1*X3	1	55.125	55.125	13.73
X2*X3	1	78.125	78.125	19.46
Error	25	16.5	0.66	
Lack-of-Fit	1	0	0	
Pure Error	24	16.5	0.6875	
Total	31	401.5		

3.3 Machine Learning-Based Predictive Analysis

The experimental impact toughness result set with 32 rows of data is used for the development of ML models by splitting it into training and testing portions. To obtain the best results, three ratios of training-testing data splits are investigated: starting with 70%-30% and then adjusting to 80%-20% and 90%-10%. The best training and testing data proportion is found through the values of MSE and R-squared from the chosen regression models for impact toughness iteratively.

3.3.1 Decision Tree Regression

The DTR model was evaluated using three training-testing splits and varying tree depths. The flowchart of the model is presented in Figure 11. The results of Table 8 prove that increasing tree depth generally improves performance but with diminishing returns. At a depth of 2, the model underfits, especially with the 90%-10% split (R^2 = -2.30). Performance improves significantly at a depth of 3, particularly with the 80%-20% split, where MSE reaches 0.58 and R^2 is 0.96. Further depth increases show little improvement, with slight overfitting at deeper levels. The 80%-20% split and a depth of 3 provided the best balance of accuracy and complexity.

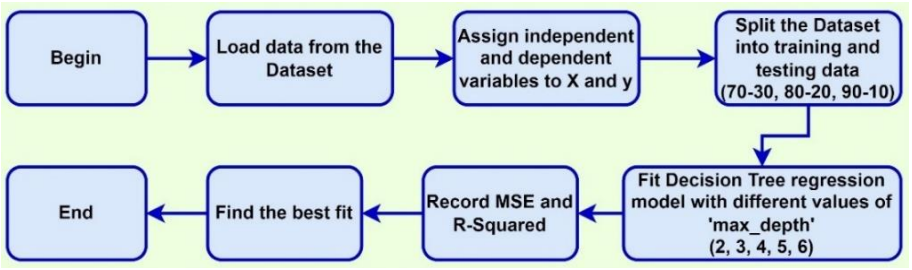

Figure 11. Flowchart of decision tree regression

Table 8. Results of the DTR

Max. Depth	Training - Testing Data Proportion					
	70%-30%		80%-20%		90%-10%	
	MSE	R-Squared	MSE	R-Squared	MSE	R-Squared
2	1.81	0.89	1.26	0.90	1.65	-2.30
3	0.67	0.96	0.58	0.96	0.88	-0.75
4	0.67	0.96	0.58	0.96	0.88	-0.75
5	0.67	0.96	0.58	0.96	0.88	-0.75
6	0.67	0.96	0.58	0.96	0.88	-0.75

3.3.2 Random Forest Regression

The RF regression model was evaluated with different training-testing splits and varying numbers of trees. The flowchart of RF Regression is presented in Figure 12 and the results of Table 9 show the best performance with 15 trees and the 80%-20% split, achieving an MSE of 0.29 and an R-squared of 0.98, explaining 98% of the variance. Lower tree counts (5 or 10) resulted in higher MSEs and lower R-squared values. Beyond 15 trees, performance plateaued, with slight overfitting in the 90%-10% split. The 80%-20% split consistently provided the best balance, making 15 trees the optimal setting for accurate, reliable predictions.

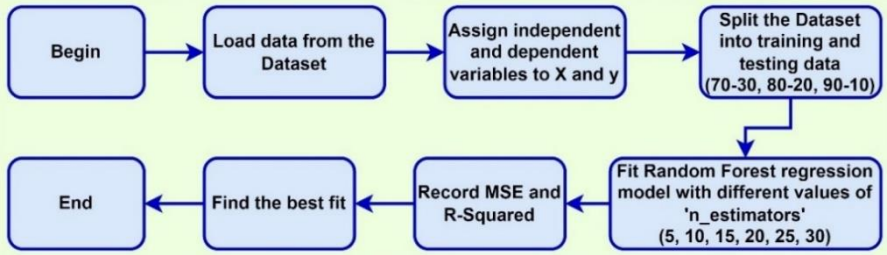

Figure 12. Flowchart of the RF model

Table 9. RF regression results

No. of Trees	Training - Testing Data Proportion					
	70%-30%		80%-20%		90%-10%	
	MSE	R-Squared	MSE	R-Squared	MSE	R-Squared
5	1.02	0.94	0.39	0.97	1.19	-1.37
10	0.57	0.96	0.32	0.98	0.77	-0.54
15	0.76	0.95	0.29	0.98	0.89	-0.77
20	0.61	0.96	0.33	0.98	0.69	-0.39
25	0.54	0.97	0.34	0.97	0.60	-0.20
30	0.69	0.96	0.35	0.97	0.64	-0.27

3.3.3 Gradient Boosting Regression

The flowchart of the implementation of GBR is presented in Figure 13 and Table 10 shows that the best performance was achieved with 20 trees and an 80%-20% split, yielding an MSE of 0.41 and an R-squared of 0.97. Lower tree counts (5 or 10) resulted in higher MSEs and lower R-squared values. Beyond 20 trees, performance gains were minimal. Gradient Boosting slightly underperformed compared to RF, especially at higher tree counts, where overfitting became more evident in the 90%-10% split. Overall, 20 trees and an 80%-20% split provided the best balance between complexity and accuracy.

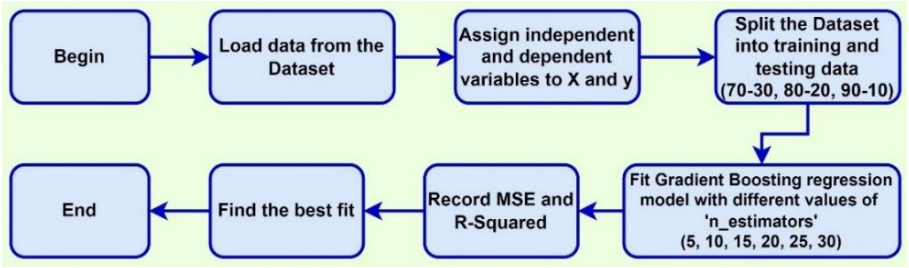

Figure 13. Flowchart of the GBR

Table 10. Results of GBR

No. of Trees	Training - Testing Data Proportion					
	70%-30%		80%-20%		90%-10%	
	MSE	R-Squared	MSE	R-Squared	MSE	R-Squared
5	5.85	0.63	4.17	0.68	2.55	-4.10
10	2.37	0.85	1.36	0.89	0.67	-0.35
15	1.20	0.92	0.57	0.96	0.34	0.33
20	0.82	0.95	0.41	0.97	0.42	0.17
25	0.70	0.96	0.42	0.97	0.55	-0.11
30	0.67	0.96	0.47	0.96	0.67	-0.33

3.3.4 Summary of the predictive results and validation

The performance of DTR, RF, and GBR models was evaluated using MSE and R-squared metrics, as summarized in Table 11. The 80%-20% training-testing split consistently provided the most accurate predictions. RF was the most accurate, with an MSE of 0.29 and R-squared of 0.98 using 15 trees, capturing non-linear relationships effectively. Gradient Boosting also performed well, with an MSE of 0.41 and R-squared of 0.97, but was slightly more prone to overfitting. Decision Tree, though simpler, yielded an MSE of 0.58 and R-squared of 0.96. Overall, Random Forest was the best model, followed by Gradient Boosting, while both outperformed Decision Tree in predictive accuracy. Table 12 compares actual impact toughness values with predictions from the three models. All models provided reasonable predictions, with Random Forest showing the closest alignment. For example, in Run 15, Random Forest predicts 26.42 J (actual: 26 J), and in Run 29, it predicts 23.90 J (actual: 24 J), demonstrating near-perfect accuracy. While Decision Tree shows slightly larger deviations (e.g., Run 23, predicted: 16 J, actual: 17 J), Gradient Boosting performs well but slightly underpredicts in some cases (e.g., Run 23). In short, Random Forest delivers the most accurate and consistent predictions, confirming the strength of ensemble methods. RF outperformed DTR and GBR because it is an ensemble approach that reduces variance by taking the average of multiple decision trees, leading to higher generalization accuracy. Unlike DTR, which tends to overfit due to its single-tree structure, RF prevents overfitting by aggregating multiple trees trained on random subsets of data. Compared to GBR, RF is less sensitive to hyperparameter tuning and mitigates overfitting better, making it more robust for predicting impact toughness.

The superior predictive accuracy of RF with 15 trees compared to 30 trees can be attributed to optimal bias-variance tradeoff, avoidance of overfitting, and computational efficiency. With 15 trees, the model stabilized and additional trees offered diminishing returns, increasing complexity without significantly improving generalization.

Table 11. Best results of MSE and R-squared values

Decision Tree			Random Forest			Gradient Boosting		
Max. Depth	MSE	R-squared	No: of Trees	MSE	R-squared	No: of Trees	MSE	R-squared
3	0.58	0.96	15	0.29	0.98	20	0.41	0.97

Table 12. Actual and predicted impact toughness values

Run	X1	X2	X3	Actual Impact Toughness (J)	Predicted Impact Toughness (J)		
					Decision Tree	Random Forest	Gradient Boosting
12	4	12	3	17	16.50	17.34	16.89
23	6	8	5	17	16.00	16.19	16.45
11	4	12	3	18	16.50	17.34	16.89
3	4	8	3	16	16.00	15.80	16.45
17	6	8	3	18	18.67	18.77	18.79
15	4	12	5	26	26.33	26.42	25.52
29	6	12	5	24	24.00	23.90	23.47

Though the minimal deviations between the experimental and predicted impact toughness in the test data (Table 12) prove the robustness of the RF model, it is further tested with unknown values of X1, X2 and X3. Thereafter, a confirmation experiment is conducted with the same inputs to check the deviation between the predicted and actual values. Table 13, which presents the results of the prediction and confirmation experiment, corroborates the validity of the RF model with a minor deviation of 1.25%.

Table 13. Results of prediction and confirmation experiment

X1	X2	X3	Impact Toughness (J)		% Deviation
			Prediction	Confirmation Experiment	
5	10	4	15.8	16	1.25

3.3.5 Scope for future work

Despite promising results in predicting the impact toughness of AISI 430-AISI 304 friction-welded joints using ML, a few limitations need further exploration. This study focused on a limited range of welding parameters (friction force, forge force, and burn-off), ignoring factors like rotational speed and cooling rate, which could significantly affect joint quality. These aspects could be explored in future works. Impact toughness investigation and prediction at elevated temperatures, which can benefit the aerospace and automotive sectors, can also be taken up. The dataset used for training

the models was relatively small, limiting the generalizability of the predictions. Additionally, mechanical characterization was restricted to impact toughness, excluding other critical properties like fatigue resistance and tensile strength. While traditional ML models performed well, advanced techniques such as deep learning or hybrid models could further improve predictive accuracy.

4. CONCLUSIONS

This study evaluated and predicted the impact toughness of dissimilar AISI 430-AISI 304 stainless steel friction welded joints using ML techniques. Key conclusions derived from the investigation are:

i) AISI 304 austenitic stainless steel possesses lower thermal conductivity, higher hardness and superior strength compared to AISI 430 ferritic counterpart. Hence, more deformation and burn-off flash is generated on the AISI 430 side during friction welding, which is why the joint exhibited impact toughness that is more aligned towards AISI 430. The microstructural differences, including parallel bands on the austenitic side and equiaxed grains on the ferritic side, were influenced by dynamic recrystallization during welding.

ii) The impact toughness of the welded joints ranged from 15 to 27 J, with the highest toughness achieved when the forging force was at its maximum. The heat generated by friction and its controlled distribution contributed to the microstructural stability, enhancing the toughness of the joints.

iii) The Taguchi analysis reveals that maximum impact toughness is achieved when X1, X2, and X3 are all set to their highest levels. Parameters X1, X2, and X3 contribute 0.04% to 4.17% individually, but their interactions, particularly X1*X3 and X2*X3, significantly affect the outcomes, i.e. 13.73% and 19.46%. This suggests that burn-off reduces heat from friction and forge forces, leading to increased impact toughness when these parameters are high.

iv) Among the various ML models employed, Random Forest regression (15 trees and 80%-20% data split) exhibited the highest predictive accuracy for impact toughness, with an MSE of 0.29 and R-squared value of 0.98. Predicted impact toughness from the Random Forest model and the confirmation experiment exhibited a mere 1.25% deviation, demonstrating near-perfect accuracy.

v) The predictive models minimized the need for extensive experimental testing, demonstrating the effectiveness of ML in optimizing welding parameters and predicting material behavior. This integration of ML can streamline the welding process, improving both performance and reliability in industrial applications.

vi) Even though Random Forest effectively predicted impact toughness, advanced techniques like deep learning or hybrid models could improve accuracy. The approach can be applied to other materials, and future studies should explore microstructural changes under conditions like fatigue, high temperatures, or corrosion to assess long-term durability.

ACKNOWLEDGEMENTS

The authors would like to express their sincere gratitude to the Department of Mechanical, Bioresources and Biomedical Engineering, College of Science, Engineering and Technology, University of South Africa, Florida Campus, Johannesburg, South Africa for their cooperation and support during the preparation of this work. Also, thank you to Dr. G. Madhusudan Reddy, Visiting Professor at the National Institute of Technology, Warangal, India, for the support and guidance during the execution of the research work.

CONFLICT OF INTEREST

The authors declare no conflicts of interest.

AUTHORS CONTRIBUTION

Jagadesh Kumar Jatavallabhula: Conceptualization, Investigation, Data Curation, Writing - Original Draft.

Vasudeva Rao Veeredhi: Validation, Resources, Supervision.

Gundeti Sreeram Reddy: Project administration, Writing - Review & Editing.

Ravinder Reddy Baridula: Data Curation, Methodology, Writing - Original Draft.

Vaddi Venkata Satyanarayana: Conceptualization, Formal analysis, Writing - Review & Editing.

FUNDING

This study was not supported by any grants from funding bodies in the public, private, or not-for-profit sectors.

REFERENCES

[1] Guo G, Shen Y, "Microstructure and mechanical properties of friction stir welded austenitic-ferritic stainless steels using staggered joint configuration," *Journal of Materials Engineering and Performance*, vol. 29, pp. 5263-5272, 2020.

[2] Byeong-heon Kim, Ki-hwan Kim, Young-jin Kang, Sung-shin Kim, Hee-je Kim, "Hastelloy C276/AISI SS304 dissimilar metal welding: A comparative review of the effective application of laser and Micro-GTAW," *Journal of Materials Research and Technology*, vol. 32, pp. 621-633, 2024.

[3] H. T. Serindağ and G. Çam, "Microstructure and mechanical properties of gas metal arc welded AISI 430/AISI 304 dissimilar stainless steels butt joints," *Journal of Physics: Conference Series*, vol. 1777, no. 1, p. 012047, 2021.

[4] S. Emami, S. Sadeghi-Kanani, T. Saeid, and F. Khan, "Dissimilar friction stir welding of AISI 430 ferritic and AISI 304L austenitic stainless steels," *Archives of Civil and Mechanical Engineering*, vol. 20, no. 131, pp. 1-16, 2020.

[5] G. M. Reddy and K. S. Rao, "Microstructure and mechanical properties of similar and dissimilar stainless steel electron beam and friction welds," *Int. J. Adv. Manuf. Technol.*, vol. 45, pp. 875-888, 2009.

[6] Y. I. Karlina, R. V. Kononenko, V. V. Ivancivskiy, M. A. Popov, F. F. Deryugin, and V. E. Byankin, "Overview of modern requirements for welding of high-strength low-alloy pipe steels," *Processing of Metals*, vol. 25, no. 4, pp. 36-60, 2023.

[7] A. Zambrano, "A review on the effect of impact toughness and fracture toughness on impact-abrasion wear," *Journal of Materials Engineering and Performance*, vol. 30, no. 10, pp. 7101-7116, 2021.

[8] K. Kim, M. Park, J. Jang, H. C. Kim, H.-S. Moon, D.-H. Lim, J. B. Jeon, S.-H. Kwon, H. Kim, and B. J. Kim, "Improvement of strength and impact toughness for cold-worked austenitic stainless steels using a surface-cracking technique," *Metals*, vol. 8, no. 11, p. 932, 2018.

[9] Z. L. Hou, H. Q. Guo, J. J. Wang, Z. Y. Huang, Z. A. Wang, D. S. Fang, and J. Qiao, "Research on the low-temperature impact toughness of a new 100-mm ultra-thick offshore steel fabricated using the narrow-gap laser wire filling welding process," *Materials*, vol. 17, no. 6, p. 1363, 2024.

[10] P. Luo, W. Feng, G. Zu, L. Luo, and J. Xiao, "Microstructure and impact toughness of laser-arc hybrid welded joint of medium-thick tc4 titanium alloy," *Coatings*, vol. 14, no. 4, p. 395, 2024.

[11] O. Tunçel, "Optimization of charpy impact strength of tough pla samples produced by 3D printing using the taguchi method," *Polymers*, vol. 16, no. 4, p. 459, 2024.

[12] S. S. Abdelhady, R. E. Elbadawi, and S. H. Zoalfakar, "Multi-objective optimization of FSW variables on joint properties of AA5754 aluminum alloy using Taguchi approach and grey relational analysis," *The International Journal of Advanced Manufacturing Technology*, vol. 130, pp. 4235-4250, 2024.

[13] W. Safeen, S. Hussain, A. Wasim, M. Jahanzaib, H. Aziz, and H. Abdalla, "Predicting the tensile strength, impact toughness, and hardness of friction stir-welded AA6061-T6 using response surface methodology," *International Journal of Advanced Manufacturing Technology*, vol. 87, pp. 1765-1781, 2016.

[14] Devaraj, Jeyaganesh, Aiman Ziout, Jaber E. Abu Qudeiri, Rashfa A Baalfaqih, Nasmah Baalfaqh, Kanna Alahbabi, Maitha Alnaqbi, Noura Alhosan, "Using machine learning models to predict weld sequence giving minimum distortion," *Advances in Science and Engineering Technology International Conferences (ASET), Dubai, UAE*, pp. 1-6, 2022.

[15] G. Chen, B. Sheng, R. Luo, and P. Jia, "A parallel strategy for predicting the quality of welded joints in automotive bodies based on machine learning," *Journal of Manufacturing Systems*, vol. 62, pp. 636–649, 2022.

[16] Y. Chen *et al.*, "Identifying facile material descriptors for Charpy impact toughness in low-alloy steel via machine learning," *Journal of Materials Science and Technology*, vol. 132, pp. 213-222, 2023.

[17] S. Wei Wu, J. Yang, and G. Ming Cao, "Prediction of the Charpy V-notch impact energy of low carbon steel using a shallow neural network and deep learning," *International Journal of Minerals, Metallurgy and Materials*, vol. 28, no. 8, pp. 1309-1320, 2021.

[18] Y. Diao, L. Yan, and K. Gao, "A strategy assisted machine learning to process multi-objective optimization for improving mechanical properties of carbon steels," *Journal of Materials Science and Technology*, vol. 109, pp. 86-93, 2022.

[19] M. Shaban, M. F. Alsharekh, F. N. Alsunaydih, A.I. Alateyah, M.O. Alawad et al., "Investigation of the effect of ECAP parameters on hardness, tensile properties, impact toughness, and electrical conductivity of pure cu through machine learning predictive models," *Materials*, vol. 15, no. 24, p. 9032, 2022.

[20] J. Pak, J. Jang, H. K. D. H. Bhadeshia, and L. Karlsson, "Optimization of neural network for charpy toughness of steel welds," *Materials and Manufacturing Processes*, vol. 24, no. 1, pp. 16-21, 2009.

[21] J.F. Durodola, "Machine learning for design, phase transformation and mechanical properties of alloys," *Progress in Materials Science*, vol. 123, p. 100797, 2022.

[22] A. Stoll and P. Benner, "Machine learning for material characterization with an application for predicting mechanical properties," *GAMM - Mitteilungen*, vol. 44, p. e202100003, 2021.

[23] K. Guo, Z. Yang, C.-H. Yu, and M. J. Buehler, "Artificial intelligence and machine learning in design of mechanical materials," *Materials Horizons*, vol. 8, no. 4, pp. 1153-1172, 2021.

[24] M. Smyrnov, F. Funcke, and E. Kabliman, "Prediction of material toughness using ensemble learning and data augmentation," *Philosophical Magazine Letters*, vol. 104, no. 1, p. 2372497, 2024.

[25] G. Xu, X. Zhang, and J. Xu, "Data augmentation of micrographs and prediction of impact toughness for cast austenitic steel by machine learning," *Metals*, vol. 13, no. 1, p. 107, 2023.

[26] Z. Sabouri, N. Gherabi, and M. Amnai, "Comparative study of supervised regression algorithms in machine learning," in *Advances in Intelligent System and Smart Technologies*, N. Gherabi, A. I. Awad, A. Nayyar, and M. Bahaj, Eds. Cham, Switzerland: Springer, vol. 826, pp. 365-374, 2024, *Lecture Notes in Networks and Systems*.

[27] Costa, V.G., Pedreira, C.E., "Recent advances in decision trees: an updated survey," *Artificial Intelligence Review*, vol. 56, pp. 4765-4800, 2023.

[28] Iranzad, R., Liu, X., "A review of random forest-based feature selection methods for data science education and applications," *International Journal of Data Science and Analytics*, vol. 2024, pp. 1-15, 2024.

[29] Bentéjac C, Csörgő A, Martínez-Muñoz G, "A comparative analysis of gradient boosting algorithms," *Artificial Intelligence Review*, vol. 54, pp. 1937-1967, 2021.

[30] Hosseinpoor S, Sheikhmohammadi A, Rasoulzadeh H, Saadani M, Ghasemi SM, Alipour MR, Hadei M, Zarch SM, "Comparison of modeling, optimization, and prediction of important parameters in the adsorption of cefixime onto sol-gel derived carbon aerogel and modified with nickel using ANN, RSM, GA, and SOLVER methods," *Chemosphere*, vol. 353, p. 141547, 2024.

[31] Jian Gao, "R-Squared (R^2) – How much variation is explained?" *Research Methods in Medicine & Health Sciences*, vol. 5, no. 4, pp. 104-109, 2024.

[32] Prateek, S., Garg, R., Kumar Saxena, K., Srivastav, V. K., Vasudev, H., Kumar, N., "Data-driven materials science: application of ML for predicting band gap," *Advances in Materials and Processing Technologies*, vol. 10, no. 2, pp. 708-717, 2023.

[33] Chu, T.K., Ho, C.Y., "Thermal conductivity and electrical resistivity of eight selected AISI stainless steels," *Thermal Conductivity 15*, pp. 79-104, Springer, 1978.

[34] V. Ajay, N. Kishore Babu, M. Ashfaq, T. Mahesh Kumar, K. Vamsi Krishna, "A review on rotary and linear friction welding of inconel alloys," *Transactions of the Indian Institute of Metals*, vol. 74, pp. 2583-2598, 2021.

[35] A. Atamashkin, E. Priymak, E. Tulibaev, Y. Syomka, and V. Trushov, "Influence of force parameters of rotary friction welding on the microstructure and mechanical properties of welded joints of high-strength drill pipes," *International Journal on Interactive Design and Manufacturing (IJIDeM)*, vol. 15, no. 6, pp. 1-13, 2024.